PIAVE SUPER-CONDUCTING INJECTOR 2

In 1996 the Legnaro accelerator complex consisted in a XTU tandem followed by the super-conducting linear booster ALPI. It delivered ion beams to the experimental rooms with beam intensities on the target of few pnA, masses ranging from protons to masses of the order of $A = 100$ (^{81}Br) and energies well above the Coulomb barrier. The main constraint for the existing facility was the presence of the stripping section inside the tandem that limited the performance of the accelerator complex towards the heavier masses, up to $A = 200$, and the beam intensities. On the other hand the nuclear physicists were moving their interests to the very heavy ion beams with energies around the interaction barrier. As a consequence of this request, a new injector for the ALPI booster was proposed at the beginning of 1996.

In mid 2006 the injector was fully commissioned and a complete characterization of the beam out of the injector was finally obtained. With these parameters it was possible to derive for the first time the ideal best performances of PIAVE-ALPI accelerator complex.

2.1 PIAVE: a brief description

The injector PIAVE (Positive Ion Accelerator for Very low Energy) was meant for increasing the mass range of the facility up to Pb [1] and it was designed to accelerate ions with $A/q \leq 8.5$ up to 1.2 MeV/A. The main components are an ECRIS source operating on a high voltage platform, a three harmonic buncher, a super-conducting RFQ cryomodule containing two bulk niobium structures and two QWR cryomodules housing 4 cavities each.

The commissioning with various beam species of the low-energy beam transport before the SRFQs was competed in 2000 [2] and the commissioning of SRFQs and QWRs in early spring 2006 [3]. Starting from October 2006, the nuclear physics experiments with PIAVE Injector have been scheduled by the international Programme Advisory Committee.

The injector setup started in November 2004 with a $^{16}O^{3+}$ pilot beam. In December 2005, after a long shutdown of the ALPI booster cryogenic plant, a very first ^{22}Ne test beam was accelerated by PIAVE and ALPI to the experimental apparatus PRISMA-Clara (final energy ~ 6 MeV/A), where it provided stable beam-on target conditions for around 50 hours, before scheduled conclusion.

In the period January-April 2006, the LNL TANDEM-ALPI operation programme allotted around 5 days/month for PIAVE-ALPI beam tests. In this period, tests with ^{22}Ne, ^{132}Xe, ^{40}Ar and ^{84}Kr beams were conducted. Final energy on target ranged between 5 and 8.25 MeV/A and currents between 5 and 15 pnA. The typical time required driving the beam through injector and booster to the experimental station was ~ 36 hours.

2.1.1 The line before the SRFQs

PIAVE injector uses the beams generated by the ECR Ion Source ALICE placed on a high voltage platform operated at 350 kV [4], with the possibility of implementing a 5 MHz pulsing system for TOF measurements in the future. Ion source beam, extracted with a typical $V_s = 11$ kV

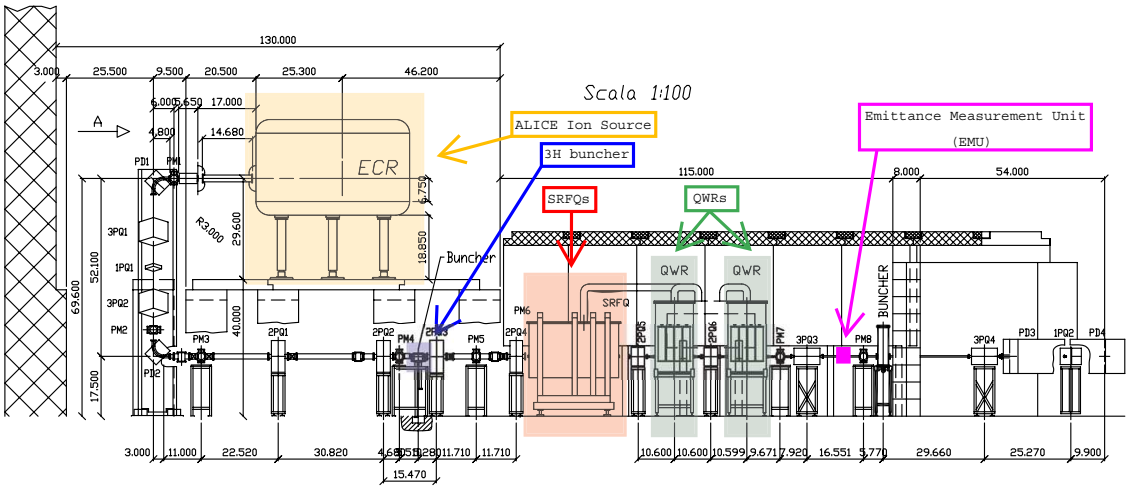

Figure 2.1: PIAVE layout.

voltage (total current I_s = 0.5 mA), is mass separated (resolving power $m/\Delta m$ = 100) and finally accelerated by electrostatic column up to the nominal β = 0.00892 for RFQ injection. For a typical $^{132}Xe^{18+}$ beam (A/q = 7.33), the platform voltage is set to V_p = 270 kV with 17 V ripple. Production of beams from metallic elements ($^{63}Cu^{11+}$, $^{107}Ag^{18+}$, $^{120}Sn^{19+}$) has been demonstrated [5].

Following the accelerating column (see Fig. 2.1), the line is composed by an achromatic bend, a couple of doublets that focuses the beam at the buncher, followed by the second couple of doublets needed for the matching at the RFQ input.

After the analysis of different options, a three harmonics buncher was selected, with 40 MHz as fundamental frequency, at a distance of 3.51 m from the RFQ input. Indeed, since for each harmonic a two gaps configuration is used, the first and the third harmonics are applied in a first buncher, the second harmonic in a second buncher at a distance of 120 mm; all voltages are below 4 kV[6] [7]. The design efficiency of the bunching is such that 70 % of the particles are captured by the RFQ with a final RMS longitudinal emittance of 0.13 ns keV/A with nominal focusing. Simpler configurations, like double drift double frequency bunchers, have not the same performances, due to the fixed distance between the two bunchers and the consequent difficulty of getting small beam waists in all gaps.

2.1.2 The super-conducting RFQ

The heart of PIAVE injector [8] is the super-conducting RFQ section. The main design parameters are summarized in Tab. 2.1. The SRFQ, without a complete bunching section, was optimized to achieve a high accelerating gradient, since power losses are negligible and the cost of the structure and associated cryostat is rather high. This result was obtained by splitting the RFQ in two independent cavities. In SRFQ2, thanks to the increased beta, both the intervane voltage V and the aperture R0 are almost doubled. In this second structure (with V = 280 kV) the accelerating field exceeds 2.8 MV/m, which is the world record for an RFQ, and the normalized transverse acceptance exceeds 2.5 mm mrad.

The two SRFQ resonators are of ladder kind, with four stems per electrode in SRFQ1 and two in SRFQ2; the transverse dimensions are therefore almost the same. The field configuration of the operating mode in these resonators is pretty insensitive to geometric errors, since in the worst case the resonator length is 0.37 λ and the dipoles are 10 MHz higher in frequency. It is instead very critical the tuning of the operating mode frequency (starting from an achieved mechanical accuracy better than 50 μm in the welded assembly) and the stiffening of the system against vibrations.

Table 2.1: Original PIAVE specifications.

parameter	base value		unit	comment
Source and LEBT				
Ion source	14.5		GHz	ECRIS
max A/q	8.5			for $^{238}U^{28+}$
max platform voltage	315		kV	
rms emittance	0.1		mm mrad	normalized
bunching system	40; 80; 120		MHz	three harmonics
$\Delta\phi$	± 6		deg	@ 80 MHz
ΔW	± 0.55		keV/A	
RFQ Accelerator				
Radio Frequency	80		MHz	
input energy	37.1		keV/A	β = 0.0089
output energy	586		keV/A	β = 0.0355
max surface field	25		MV/m	
max stored energy	≤ 4		J	each RFQ
acceptance	≤ 0.9		mm mrad	normalized
	0.1		mm mrad	normalized
	≤ 0.14		ns keV/A	
	SRFQ1	*SRFQ2*		
Vanes length	137.8	74.61	cm	
Output energy	341.7	586	keV/A	
max voltage	148	280	kV	
number of cells	42.6	12.4		
average aperture R0	0.8	1.53	cm	
modulation factor m	1.2-3	3		
synchronous phase	-40 ÷ -18	-12	deg	
QWR section				
number of resonators	8			
output energy	948		keV/A	β = 0.045
radio fequency	80		MHz	
optimum β	0.05			
accelerating field	3		MV/m	
shunt impedance	3.2		kΩ/m	
synchronous phase	-20		deg	
Matching line to ALPI				
number of bunchers	2			room temperature
buncher eff. voltage	≤100		kV	VT

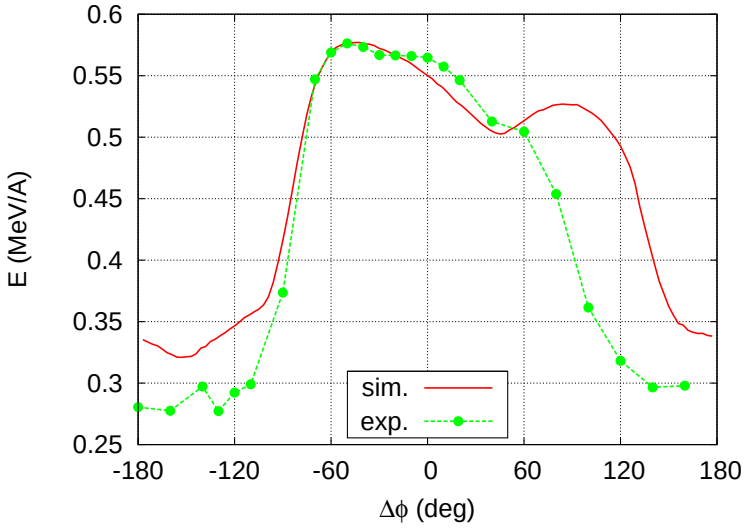

Figure 2.2: Simulated and measured energy in the case of $^{16}O^{3+}$ at SRFQs exit as function of the phase of SRFQ2.

The physical distance between the two SRFQs (200 mm) determines a transverse beam mismatch in SRFQ2 (where the acceptance is large). This mismatch was minimized interrupting SRFQ1 in a point where the Twiss parameter are $\alpha_x = \alpha_y = 0$. Longitudinally instead the phase advance is matched with the correct choice of the synchronous phase of SRFQ2. Moreover in the transition region one can profit of an additional acceleration specific of these alternating stem structures [9].

2.1.3 The line after the SRFQs

Following the SRFQ (at $\beta = 0.355$) the beam enters directly in the QWR section. The structure of this accelerator section follows the ALPI scheme, four resonators per cryostat, but for the transverse focussing period the lattice is, in this case, made of quardupole doublets and no diagnostic boxes between the two cryostats. Therefore one can use an accelerating gradient of 5 MV/m giving more margins for proper injection in ALPI.

The main difference between these resonators and the ALPI low-β resonators is that the inner conductor is squeezed to decrease the distance between the gaps to optimize the structure for the lower velocity (PIAVE $\beta_o = 0.047$, ALPI $\beta_o = 0.055$). The required accelerating electric field of PIAVE QWR was increased from 3 MV/m at 7 W to 5 MV/m following the very good results of the first prototype. At present, the average accelerating field of all cavities is 6.8 MV/m with 7 W.

The longitudinal matching between the SRFQs and the QWRs section is achieved using the first cavity as a buncher, and with alternating phase focusing. The synchronous phase sequence is (-90, +20, +20, +20, -20, -20, +20, +20). This approach allows a compact system, but it is sensitive to alignment errors that can easily result in important longitudinal emittance increase.

To transport the beam from the exit of the accelerating structure of PIAVE to the entrance of ALPI a Medium Energy Beam Transport (MEBT) line is foreseen. This MEBT is about 10 m long and includes two quadrupole triplets, two room temperature bunchers and one magnetic L-bend, made of two 45° dipoles separated by one quadrupole singlet for the chromaticity correction.

2.2 PIAVE SRFQs commissioning

Beam tests were carried out in three steps, with different positions of a temporary emittance measuring unit (EMU): at the SRFQ input [2], after the SRFQ [10] and after the QWRs. The EMU contains two slit and harp BPM (44 channels) systems moving along x and y direction, a FC and a Si detector. In addition PIAVE is equipped with 8 permanent measurement positions, with harp

BPM and FC. Finally, in the third commissioning phase the beam could be transported after the first 45° dipole of the bend to ALPI (with NMR field measurement) and analyzed in energy.

The two PIAVE SRFQs have been tuned with $^{16}O^{3+}$ beam and the external buncher off, recording beam transmission (on FC) and energy spectrum (on Si detector) for different phases of SRFQ2 (Fig. 2.2); a current of $\sim 1 \div 3$ μA was typically available from the source. It should be noted that the quadrupole doublet 2PQ5, located after the SRFQs and before the EMU, determines a certain energy selection due to chromaticity. This effect is taken into account in the PAMTEQM-PARMILA simulations superimposed to the measurements in Fig. 2.2. Simulations and measures match very well in the phase range in which the SRFQ1 beam falls within the SRFQ2 separatrix, allowing a precise determination of the nominal SRFQ2 phase.

After this phase regulation, the buncher has been switched on to the nominal voltages and adjusted in phase so to reach the maximum transmission. The values of transmission reached in January 2005 were in the 40-45% region, in disagreement with simulations that predicted a 68%. It was hence decided to realign the LEBT respect to the RFQ, checking both with optical devices and with best beam transmission. At the end of this process, the beam transmission predicted by simulations was achieved.

2.2.1 Transverse emittance measurements

After phase tuning, the SRFQs have been completely characterized through a set of transverse and longitudinal emittance measurements for different beams. In Tab. 2.2 the results for $^{40}Ar^{9+}$ and $^{16}O^{3+}$ after the RFQ are presented. These values are perfectly consistent with LEBT beam measurements and RFQ simulations.

Ion	$\varepsilon_{RMS,\,x}$	$\varepsilon_{RMS,\,y}$
$^{40}Ar^{9+}$	0.10	0.10
$^{16}O^{3+}$	0.11	0.12
$^{40}Ar^{9+}$ @ 1.2 MeV/A	0.13	0.20

Table 2.2: Transverse emittance measurements out of PIAVE SRFQs. The values are in [mm.mrad] and are normalized.

2.2.2 Longitudinal emittance measurements

Longitudinal emittance has also been measured in the same position, using a silicon detector intercepting the particles scattered at 25° angle by a thin golden foil. The data acquisition system allows to determine the time-energy correlations with the possibility (in principle) to get a direct plot of the longitudinal emittance. In practice, while the bunch length measured seems correct, an acceptable energy resolution cannot be achieved. The comparison of the energy spread of an Ar beam after the RFQ as foreseen by simulations, as measured with silicon detector and as measured with magnetic dispersion after the dipole PD3 indicates that the silicon detector overestimates of an order of magnitude the energy spread. The spread from simulation is $\Delta W/W = 0.3$ %, while Si measurement gives $\Delta W/W = 9.0$ % and magnetic dispersion $\Delta W/W = 0.6$ %.

Table 2.3: Longitudinal emittance measured using $^{36}Ar^{9+}$ beam.

method	ε_z (deg MeV / A @ 80 MHz)	ε_z (keV ns)
Si detector	39.0 ± 1.6	1.358 ± 0.006
3 gradients	4.8 ± 0.2	0.17 ± 0.01
simulated	2.2	0.08

As a consequence the RMS emittances measured with time-energy correlation of Si detector signals are overestimated. Therefore it was decided to measure the longitudinal emittance indirectly, following the three gradients method described below. This method gives an emittance value that is within a factor 2.5 in agreement with what expected from simulations for a perfectly aligned machine (see Tab. 2.3). This result is encouraging and shows that the SRFQ can give a longitudinal emittance perfectly comparable with the performances of the other heavy ion injectors.

3 gradients method

With the 3 gradients method is possible, in principle, to determine the RMS emittance in one plane just measuring the RMS width 3 times according to different settings of the line before. This would apply to the transverse plane with the beam RMS width changing the gradient of a quadrupole and to the longitudinal plane with the RMS phase width and 3 different E_{acc} of a buncher.

For the emittance measurements in PIAVE, the third cavity of the first cryostat (QWR-1.3) was used in bunching mode (synchronous phase set to -90 deg and accelerating field lower than 0.5 MV/m): this way it was possible to have the smallest waist at EMU with negligible RMS emittance increase, as shown in Fig. 2.4.

The transfer matrix for the longitudinal plane between the SRFQs out and the EMU is

$$R_z(VT) = \begin{pmatrix} 1 & L_2 \\ 0 & 1 \end{pmatrix} \begin{pmatrix} 1 & 0 \\ 0 & -\frac{2\pi}{m_0\beta^2\lambda}\frac{q}{A}\,VT \end{pmatrix} \begin{pmatrix} 1 & L_1 \\ 0 & 1 \end{pmatrix},$$

where $L_1 = 1.9$ m is the distance from the SRFQs output to the cavity and $L_2 = 5$ m from the cavity to the EMU.

In order to calculate both the Twiss parameter (α_z, β_z) and the RMS emittance ε_z at SRFQ output, one needs to know the dependence of the squared RMS phase width on the equivalent voltage VT of the cavity.

The longitudinal σ matrix of the beam at one place is

$$\sigma(\alpha_z, \beta_z, \varepsilon_z) = \begin{pmatrix} \beta_z\,\varepsilon_z & -\alpha_z\,\varepsilon_z \\ -\alpha_z\,\varepsilon_z & \frac{1+\alpha_z^2}{\beta_z}\,\varepsilon_z \end{pmatrix},$$

and therefore $\sigma_{1,1} = \beta_z\,\varepsilon_z = \phi^2_{RMS}$.

Transporting the beam backwards from the EMU to the SRFQs output this way

$$\sigma'(\alpha_z, \beta_z, \varepsilon_z) = T^{-1} \cdot R_z(VT) \cdot (T \cdot \sigma(\alpha_z, \beta_z, \varepsilon_z) \cdot T) \cdot R_z(VT)^T \cdot T^{-1},$$

where

$$T = \begin{pmatrix} -\frac{\beta\,\lambda}{360} & 0 \\ 0 & -\frac{\gamma}{(\gamma+1)\,E\,1000} \end{pmatrix}$$

is the matrix which converts the longitudinal σ matrix in MeV.deg units to mm.mrad units, $\sigma_{1,1}$ results to be a quadratic function of VT:

$$\sigma_{1,1} = \varepsilon_z \cdot (a\,(\alpha_z, \beta_z)\,VT^2 + b\,(\alpha_z, \beta_z)\,VT + c\,(\alpha_z, \beta_z)).$$

To obtain the Twiss parameters and the RMS emittance one has to fit the squared RMS phase data (the data acquisition was made via FWHM phase then converted to RMS using $\phi_{RMS} = \phi_{FWHM}/2.36$) obtained spanning the VT around the minimum of the phase. The parabola parameters by the fit are reported in Tab. 2.4.

Hence the Twiss parameters are calculated numerically inverting the system and the results are reported in Tab. 2.5.

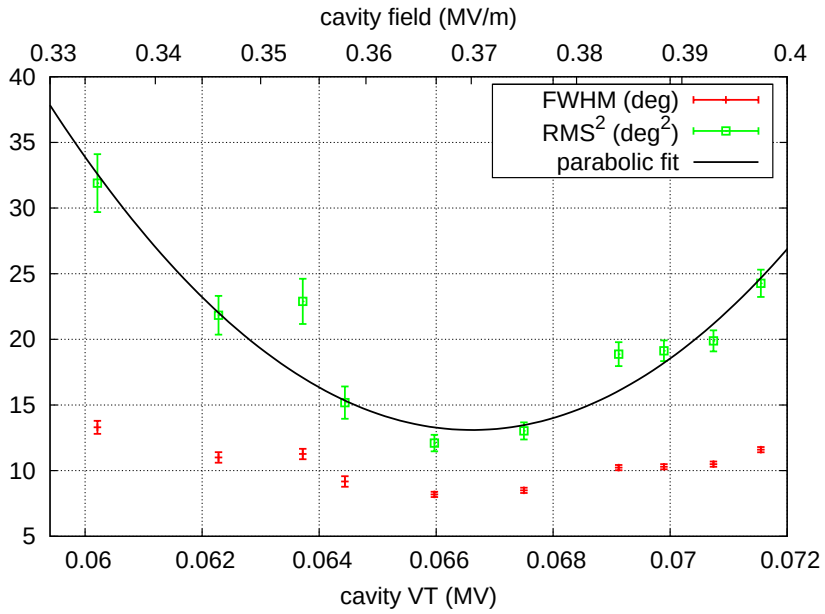

Figure 2.3: The 3 gradients method emittance measurement. Phase width at EMU.

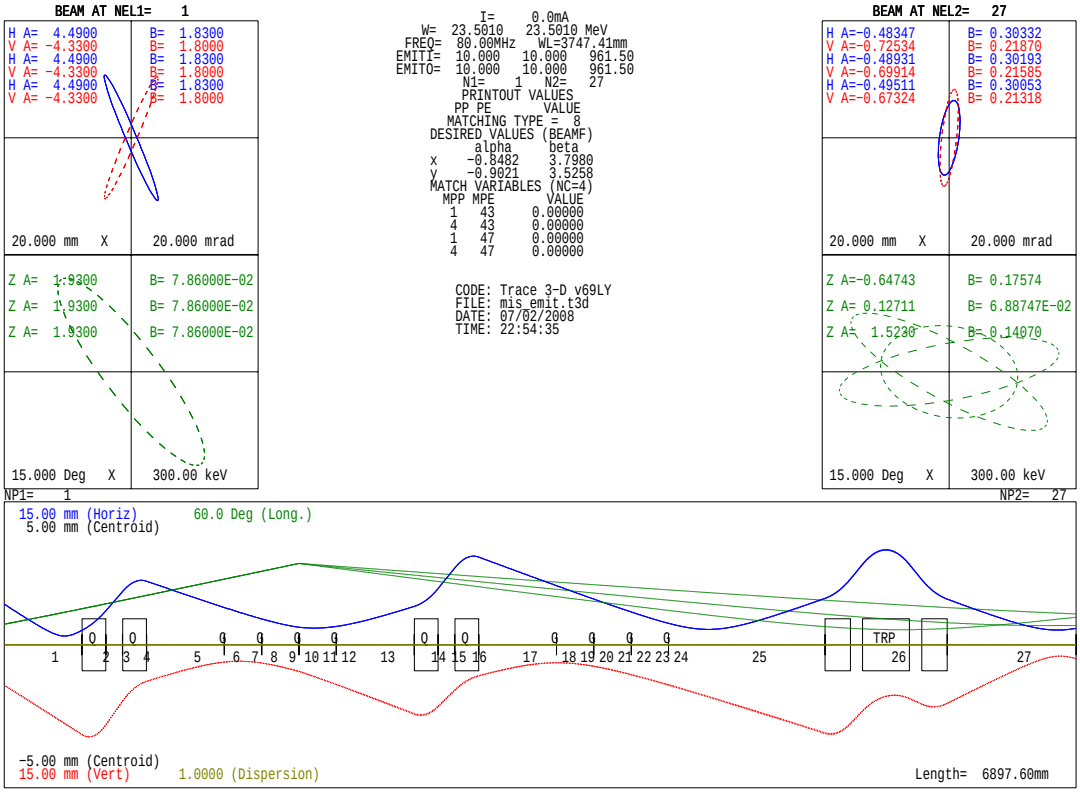

Figure 2.4: Trace3D 3 gradients longitudinal emittance plot for $VT = 0.60$ MV, $VT = 0.66$ MV (minimum) and $VT = 0.72$ MV.

Table 2.4: The parabola fitting parameters for the 3 gradients method.

fit parameters	value	rel. error
$\varepsilon_z\ a\ (\alpha_z, \beta_z)$	$(47.5 \pm 6.9) \times 10^4$	15 %
$\varepsilon_z\ b\ (\alpha_z, \beta_z)$	$(-63.3 \pm 9.2) \times 10^3$	15 %
$\varepsilon_z\ c\ (\alpha_z, \beta_z)$	$(21.2 \pm 3.2) \times 10^2$	15 %

Table 2.5: Longitudinal beam parameters out of PIAVE SRFQ.

long. parameters	value	unit	rel. error
α_z	1.93 ± 0.15		7.8 %
β_z	3.14 ± 0.16	deg / MeV / A @ 80 MHz	5.3 %
ε_z	4.81 ± 0.22	deg MeV / A @ 80 MHz	4.5 %

2.3 Improvements on PIAVE beam dynamics

Once the beam characterization of the SRFQs output was completed, it was possible to simulate the beam through the downstream line with better accuracy. In particular it was found that the original phase setting produced a considerable emittance growth both in the vertical plane (+40%) and in the longitudinal (+300%): many particles populate the low energy tails (see Fig. 2.5) and only 90% of the beam is within the limits of $-45 \leq \Delta\phi \leq +45$. The remaining 10% of the beam, even if not in PIAVE, is lost in the L-bend and in ALPI. These values were confirmed experimentally, by both a transverse emittance measurements (see Tab. 2.2) and the transmission data obtained during the shifts.

A new beam dynamics (in Tab. 5.3) was therefore studied with the aim of reducing the emittance growth. To better preserve the longitudinal distribution, larger acceptance is provided in the first cryostat using larger synchronous phases and lower accelerating fields. To recover the final energy, higher E_{acc} values are used in the second cryostat. This longitudinal "funnel" shape beam dynamics produces a slight improvement on the transverse planes whereas the longitudinal losses are reduced by 10% (see Tab. 2.7).

The comparison between the beam envelopes of the two solutions is shown in Fig. 2.6.

Table 2.6: PIAVE beam dynamics comparison. The accelerating fields E_{acc} in [MV/m] are referred to the $A/q = 7$ case and the energy E is expressed in [MeV/A].

QWR	original			present		
	E_{acc}	ϕ_s	E	E_{acc}	ϕ_s	E
1.1	2.6	-90	0.588	2.9	-90	0.588
1.2	4.1	+20	0.674	3.2	+60	0.623
1.3	4.1	+20	0.767	4.1	+30	0.706
1.4	4.1	+20	0.863	4.1	-25	0.797
1.5	4.1	-20	0.961	4.5	-20	0.891
1.6	4.1	-20	1.060	4.5	-20	0.987
1.7	4.1	+20	1.159	4.5	-20	1.084
1.8	4.1	+20	1.258	4.5	+20	1.180

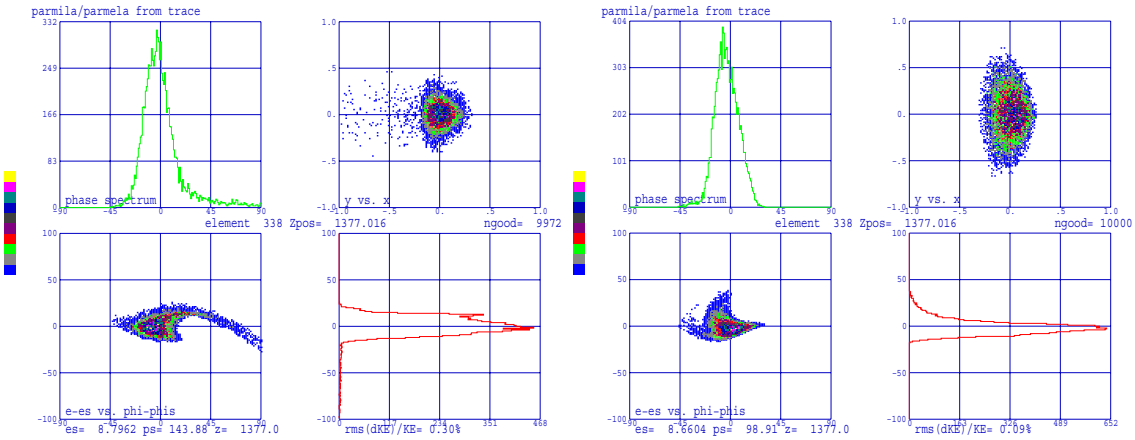

(a) Original beam dynamics. (b) Present beam dynamics.

Figure 2.5: Beam distributions at the center of the L-bend.

Table 2.7: Comparison between PIAVE original and present layout beam dynamics results.

	SRFQ out	original PIAVE	present PIAVE	unit	*var.*
$\varepsilon_{x\ rms}$	0.100	0.109	0.102		*-6%*
$\varepsilon_{y\ rms}$	0.100	0.143	0.133	mm mrad n.	*-7%*
$\varepsilon_{z\ rms}$	0.055	0.133	0.121		*-9%*
E	0.059	1.258	1.180	MeV/A	*-6%*
transm. $(-45 \leq \Delta\phi \leq +45)$		91	100	%	*+10%*

2.4 Performances of PIAVE-ALPI complex

As explained in Chapter 1, ALPI comprises at the present 3 cryostats (12 QWRs) of low-β cavities (max E_{acc} = 3.5 MV/m), 11 cryostats (44 QWRs) of medium-β cavities (max E_{acc} = 4.2 MV/m) and 2 cryostats (8 QWRs) of high-β cavities (max E_{acc} = 5.5 MV/m), for a total of 64 cavities and a voltage of 48 MV.

Only a careful longitudinal beam dynamics optimization can guarantee to exploit this voltage minimizing losses and emittance growth. For this reason a systematic study of the performances of PIAVE-ALPI as function of A/q was carried out following the results obtained with the present PIAVE beam dynamics: the use of larger synchronous phases and low E_{acc} at the beginning of the acceleration to produce a smooth focusing distributed over many cavities.

The simple ±20 choice of the synchronous phases in the low-energy branch was dropped in favor of (-90,~,+50,+40) for CR04, ±35 for CR05-06 and ±30 for CR07-10. The CR04.2 cavity is set to off because the nominal beam dynamics is studied so to have CR04.2 working in case one o is off due to failures. All the cavities of the high-energy branch are used at maximum field and at ±20 of synchronous phase.

As reported in Fig. 2.7, the E_{acc} values for 6 ≤ A/q ≤ 7 are set to 3.5 MV/m, whereas the medium-β cavities can not be set to more than 4.0 MV/m. A soft scaling is used for 5 ≤ A/q ≤ 6 and for A/q < 5 the linear A/q scaling is used. The final energies are almost linearly distributed from 10 to 6 MeV/A for 4 ≤ A/q ≤ 7 respectively.

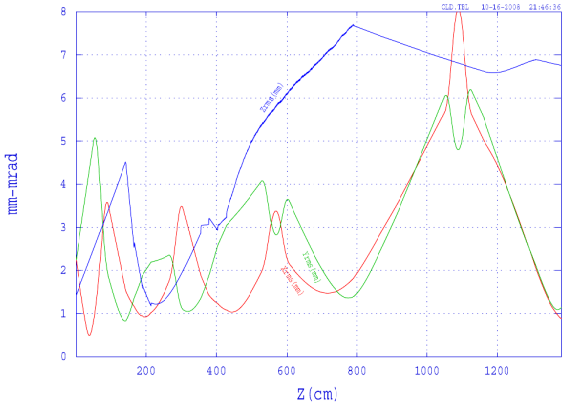

(a) Original PIAVE RMS envelopes.

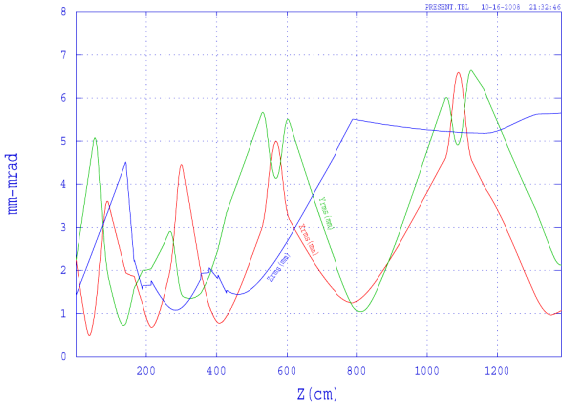

(b) Present PIAVE RMS envelopes.

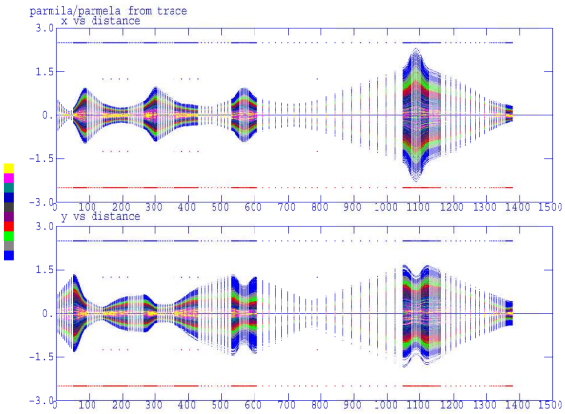

(c) Original PIAVE transverse envelopes.

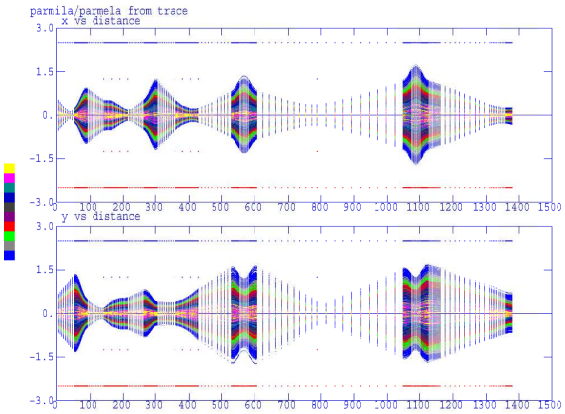

(d) Present PIAVE transverse envelopes.

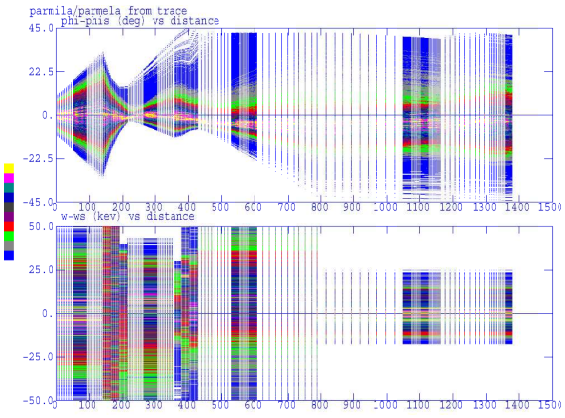

(e) Original PIAVE longitudinal envelopes.

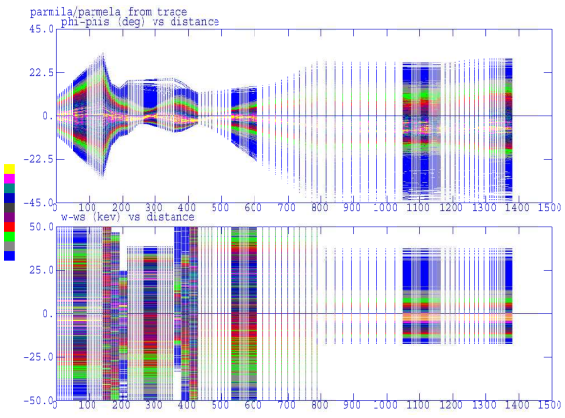

(f) Present PIAVE longitudinal envelopes.

Figure 2.6: Comparison between the original and the present PIAVE beam dynamics.

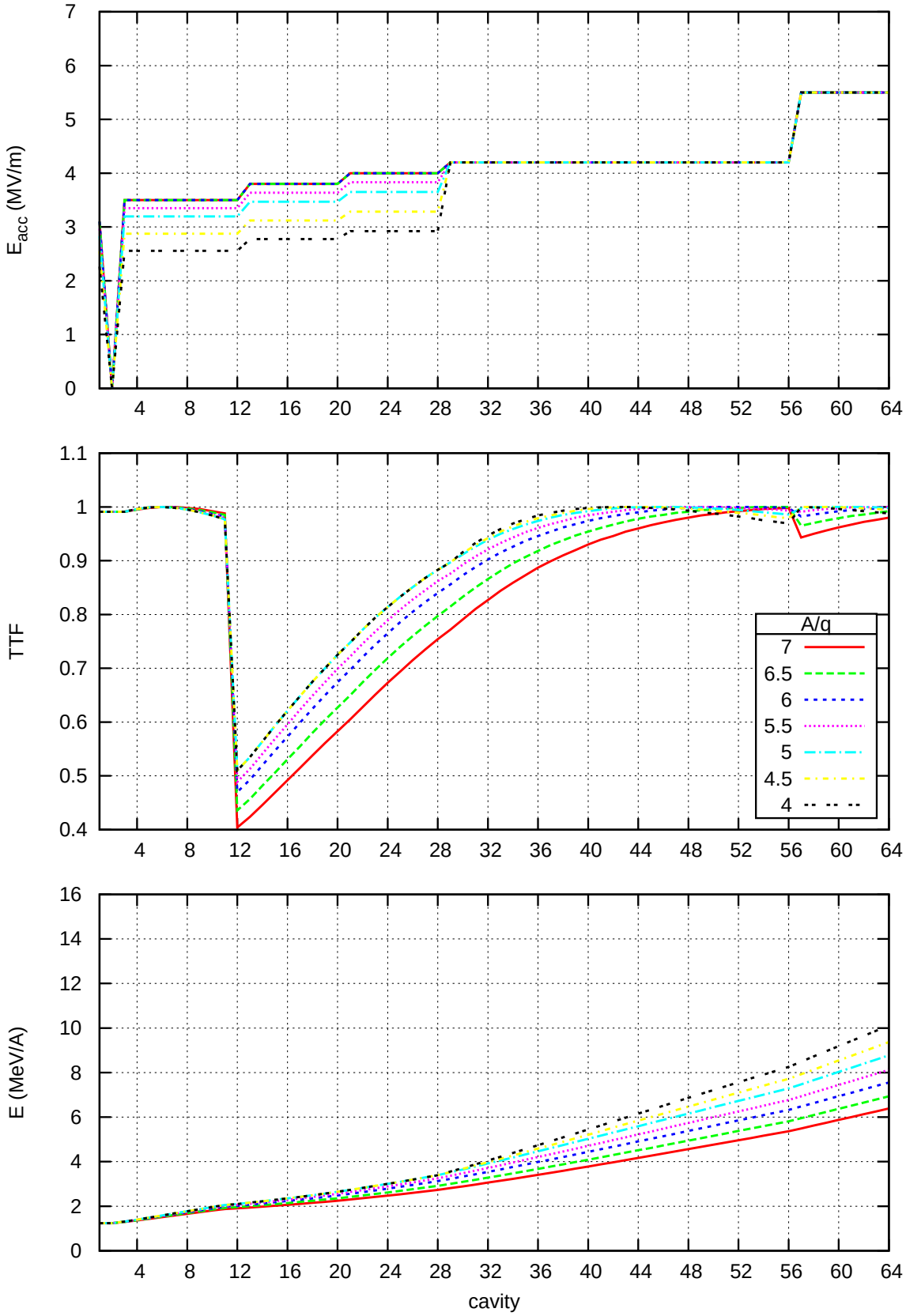

Figure 2.7: Present performances of PIAVE-ALPI complex.

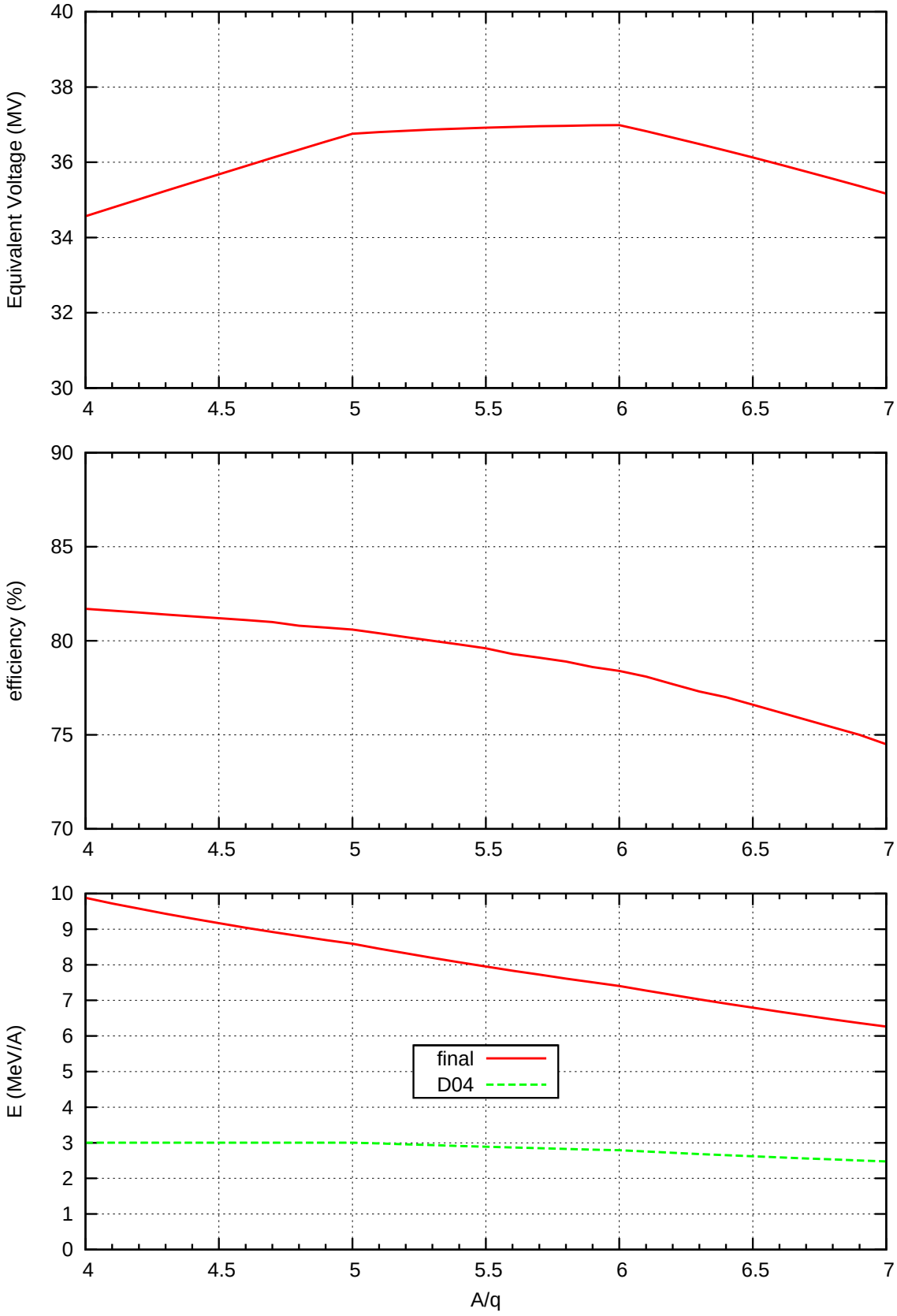

Figure 2.8: Present performances of PIAVE-ALPI complex.

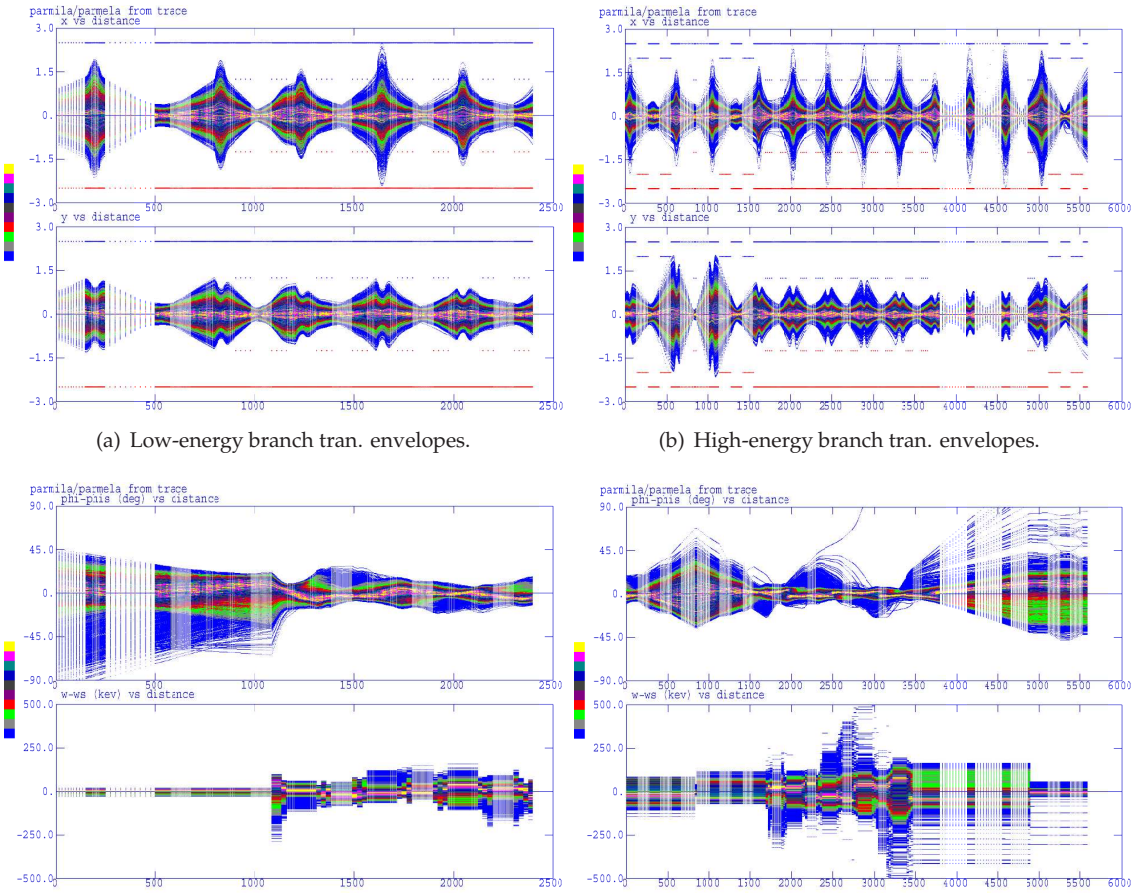

(a) Low-energy branch tran. envelopes.

(b) High-energy branch tran. envelopes.

(c) Low-energy branch long. envelopes.

(d) High-energy branch long. envelopes.

Figure 2.9: Present scenario. PARMELA simulation for A/q = 7. Transmission 97%.

Bibliography

[1] A. Lombardi and al., "The new positive ion injector PIAVE at LNL," in *Proceedings of PAC97*, (Vancouver, Canada), pp. 1129–1131, IEEE, 1997.

[2] A. Pisent, M. Cavenago, P. Bezzon, S. Canella, F. Cervellera, M. Comunian, A. Facco, A. Lombardi, and M. Poggi, "Commissioning of the LEBT of PIAVE and the ALICE ion source emittance measurement," in *Proceedings of EPAC 2000*, (Vienna, Austria), 2000.

[3] A. Pisent, G. Bisoffi, D. Carlucci, M. Cavenago, M. Comunian, A. Facco, E. Fagotti, A. Galatá, A. Palmieri, M. Poggi, A. M. Porcellato, P. A. Posocco, C. Roncolato, and S. Vitulli, "Results on the beam commissioning of the super-conducting RFQ of the new LNL injector," in *Proceedings of LINAC06*, (Knoxville (TN), USA), 2006.

[4] M. Cavenago and G. Bisoffi, "Commissioning of the ECR ion source Alice," *Nuclear Instruments and Methods A*, vol. 328, pp. 262–265, Apr 1993.

[5] M. Cavenago, A. Galatà, T. Kulevoy, S. Petrenko, M. Sattin, and A. Facco, "Refractory rf ovens and sputter probes for electron cyclotron resonance ion source," vol. 79, (Jeju, Korea), AIP, 2008.

[6] A. Facco and F. Scarpa, "The new triple harmonic buncher for the PIAVE project," in *LNL Annual Report 1996*, (Legnaro, Italy), INFN, 1996.

[7] M. Comunian and A. Pisent, "LEBT and three harmonics buncher design for PIAVE," in *LNL Annual Report 1996*, (Legnaro (PD), Italy), INFN, 1996.

[8] A. Pisent, "Design of the heavy-ion injector PIAVE," in *Proceedings of the 8th HIAT International Conference*, no. 473, (Argonne (IL), USA), AIP, 1998.

[9] A. Pisent and M. Comunian, "Complete simulation of the heavy ion linac PIAVE," in *Proceedings of PAC97*, (Vancouver, Canada), pp. 1132–1134, IEEE, 1997.

[10] A. Pisent, G. Bisoffi, D. Carlucci, M. Cavenago, F. Chiurlotto, M. Comunian, E. Fagotti, A. Galatá, T. V. Kulevoy, , M. Poggi, A. M. Porcellato, and M. Sattin, "Beam commissioning of the super-conducting RFQs of the new LNL injector PIAVE," in *Proceedings of PAC05*, (Knoxville (TN), USA), 2005.